

## Multimessenger prospects for massive black hole binaries in LISA

---

**Alberto Mangiagli<sup>a,\*</sup>**

<sup>a</sup>*Université Paris Cité, CNRS, Astroparticule et Cosmologie, F-75013 Paris, France*

*E-mail:* [mangiagli@apc.in2p3.fr](mailto:mangiagli@apc.in2p3.fr)

In  $\sim 2034$  the Laser Interferometer Space Antenna (LISA) will detect the coalescence of massive black hole binaries (MBHBs) from  $10^5$  to  $10^7$  solar mass up to  $z \sim 20$ . The gravitational wave (GWs) signal is expected to be accompanied by a powerful electromagnetic (EM) counterpart, from radio to X-ray, generated by the gas accreting on the binary. If LISA locates the MBHB merger within an error box  $< 10 \text{ deg}^2$ , EM telescopes can be pointed to detect the emission from the last stages of the inspiral or the very onset of the nuclear activity, paving the way to test the nature of gas in a rapidly changing space-time. Moreover, an EM counterpart will lead to exquisite tests on the expansion of the Universe as well as on the velocity propagation of GWs. In this talk, I present the new forecasts on the number of EM counterparts that we expect to detect over the LISA mission (Phys.Rev.D106, 103017). Starting from a population of MBHB binaries, we compute the expected EM emission under different assumptions. We find that, in the best case scenario, we expect between 7 and 20 EM counterparts in 4 yr of LISA mission. However these numbers reduce to 2-3 EMcps in 4 yr if we include obscuration and collimated radio emission. Moreover the typical galaxies hosting the GW event are faint and challenge the capabilities of future EM telescopes.

38th International Cosmic Ray Conference (ICRC2023)  
26 July - 3 August, 2023  
Nagoya, Japan



---

\*Speaker

## 1. Introduction

The Laser Interferometer Space Antenna (LISA) will observe the gravitational waves (GWs) from the coalescence of massive black hole binaries (MBHBs) up to the cosmic dawn [2]. LISA will detect systems with total mass  $M_{\text{tot}} \in [10^4, 10^7] M_{\odot}$  in the frequency range  $[10^{-4}, 10^{-1}]$  Hz. Detecting GWs from these systems will pave the way to understanding the formation and evolution mechanisms acting on MBHBs [6] as well as to perform tests of general relativity and constrain the expansion of the Universe [7, 8].

MBHBs are considered standard sirens because the GW signal carries the direction information of the luminosity distance,  $d_L$ , of the source. Therefore, if it's possible to obtain an independent estimation of the redshift, we could use MBHBs to reconstruct the  $d_L - z$  diagram and constrain cosmological parameters. The scenario where the redshift information comes from the presence of an electromagnetic (EM) counterpart is usually referred as 'bright sirens'.

At the present time, no transient-AGN like emission has been unambiguously associated to a MBHB merger. Due to the lack of observations, the possibility of an EM counterpart together with the GW signal is still unclear. The accretion of gas onto the binary can produce an EM emission during the inspiral, merger and ringdown. During the inspiral, the orbital motion of the binary is expected to excavate a cavity in the circumbinary disk and streams of gas should flow from the inner edge of the cavity to form minidisks around each MBH. In this case, the orbital motion of the binary is expected to modulate the EM emission from the minidisks, producing an EM emission that might be in phase with the GW signal. Detecting this modulation, might represent a way to identify the galaxy hosting the MBHB merger in the error volume provided by LISA [10, 11]. At or after the merger, the EM emission might appear as a powerful broadband emission, covering wavelengths from X-ray to radio [9].

Here, I present the most up-to-date forecasts for multimessenger observations. I combine the information from the sky localization provided by LISA with the sensitivities of future EM facilities under different models for the production of the EM counterpart. This proceeding is based on the work of [12].

## 2. General framework

First of all, we need a population of MBHBs as a starting point. In this work, we adopt the results of the semi-analytical models (SAM), presented in [3]. The code follows the evolution of high-redshift seed BHs across cosmic time, taking into account processes as accretion, AGN feedback and time delays. We consider three population of MBHBs: (i) Pop3: a light-seed model where BHs come from the collapse of POPIII stars, with time-delays between the galaxy and the MBHBs merger; (ii) Q3d: a heavy-seed model where BHs form from proto-galactic disks. Time-delays are included; (iii) Q3nd: same seed mechanism of the Q3d model but without time-delays. Due to the unrealistic assumption of no time-delays, this model can be viewed as an upper limit. The SAM provides the information on the number of MBHB mergers per year, the properties of the binary (i.e. masses, spins and luminosity distance) and the mass of the reservoir of gas that can accrete onto the binary and produce an EM counterpart.

For the EM counterpart, we explored three observational strategies. If the binary produce an EM counterpart in optical, the Vera C. Rubin Observatory can detect it and obtain the redshift of the host galaxy. In X-ray or radio, we do not expect any emission line and we have to rely on a complementary approach. If the binary emits in radio, the EM counterpart can be detected with the Square Kilometer Array (SKA) while the X-ray emission can be spotted by the Advanced Telescope for High ENergy Astrophysics (Athena). Once the host galaxy is identified, we get its redshift with follow-up optical observations with the Extremely Large Telescope (ELT).

When we look for an EM counterpart, the sky localization, estimated from the GW signal, is a crucial information because telescopes must be pointed in the direction of the source. Therefore we have to apply a cut in the sky localization, removing all the systems whose sky localization error is too broad to allow any realistic follow-up. This cut depends on the FOV of the telescope. For the Rubin Observatory and SKA, we select only the system with  $\Delta\Omega < 10 \text{ deg}^2$ , while for Athena we impose a cut in the sky localization at  $\Delta\Omega < 0.4 \text{ deg}^2$ . To perform the parameter estimation we use the code *lisabeta* [4].

We proceed as follow: for each MBHB merger from the SAM, we estimate its GW signal-to-noise (SNR) ratio and we select all the systems with  $\text{SNR} > 10$ . For all the systems that satisfy this requirement, we compute the EM counterpart in radio, optical and X-ray. We define *multimessenger candidate* (MMcand) any system that has  $\text{SNR} > 10$  and a detectable EM counterpart. We run the parameter estimation code on the set of MMcands to get the final information on the sky localization of the source and we define *GW event with EMcp* (EMcp) any system that is a MMcand and : (i)  $\Delta\Omega < 10 \text{ deg}^2$  if the EM emission is detectable with the Rubin Observatory or LSST or (ii)  $\Delta\Omega < 0.4 \text{ deg}^2$  if the EM counterpart is detected in X-ray (i.e. Athena).

We decide to compute the detectability of the EM counterpart before the parameter estimation of the GW signals because the latter is the most computational expensive step. In this way we can immediately discharge the events with a good sky localization and an EM counterpart too faint to be observed.

## 2.1 Modeling of the EM emission

In this section we summarise the key points necessary to compute the EM counterpart but we refer the interested reader to [12]. The starting point is the evaluation of the bolometric luminosity that can be defined as

$$\dot{M}_{\text{acc}} = \min \left( \frac{M_{\text{res}}}{t_{\nu}}, \frac{L_{\text{Edd}}}{\epsilon_{\text{rad}} c^2} \right) \quad (1)$$

$$L_{\text{bol}} = \min \left( \epsilon_{\text{rad}} \dot{M}_{\text{acc}} c^2, L_{\text{Edd}} \right) \quad (2)$$

where  $M_{\text{res}}$  is the reservoir gas mass,  $t_{\nu}$  is the viscous timescale,  $\epsilon_{\text{rad}}$  is the radiative efficiency and  $L_{\text{Edd}}$  is the Eddington luminosity

For the Rubin Observatory, we obtained the apparent magnitude  $m_{\text{AGN,Rubin}}$  applying a bolometric correction  $\text{BC} = 10$  to the bolometric luminosity. We claim that the EM counterpart is detectable if  $m_{\text{AGN,Rubin}} < 27.5$ . For the radio emission, we consider a flare and jet emission. The former is defined as

$$L_{\text{flare}} = 0.1 \epsilon_{\text{edd}} L_{\text{edd}} / q^2 \quad (3)$$

where  $\epsilon_{\text{edd}} = L_{\text{bol}}/L_{\text{edd}}$  is the Eddington ratio and  $q = m_1/m_2 > 1$  is the binary mass ratio. The latter is defined as

$$L_{\text{jet}} = \begin{cases} 0.8 \times 10^{42.7} \text{ erg s}^{-1} m_9^{0.9} \left(\frac{\dot{m}_{\text{jet}}}{0.1}\right)^{6/5} (1 + 1.1a_1 + 0.29a_1^2), & \text{if } 10^{-2} \leq \epsilon_{\text{edd}} \leq 0.3 \\ 3 \times 10^{45.1} \text{ erg s}^{-1} m_9 \left(\frac{\dot{m}_{\text{jet}}}{0.1}\right) g^2 (0.55f^2 + 1.5fa_1 + a_1^2) & \text{otherwise} \end{cases} \quad (4)$$

where  $m_9 = m_1/(10^9 M_\odot)$ ,  $\dot{m}_{\text{jet}} = \dot{M}_{\text{acc}}/(22 m_9 M_\odot \text{yr}^{-1})$ ,  $a_1$  is magnitude of the spin of the primary BH,  $f = 1$  and  $g = 2.3$  are fitting parameters. The total luminosity  $L_{\text{radio}}$  is computed as the sum of the flare and jet luminosity. The detection in radio is claimed if  $F_{\text{radio}} \geq 1.7 \times 4\pi 10^{-20} \text{ GHz } \mu\text{Jy}$  with  $F_{\text{radio}} = L_{\text{radio}}/4\pi d_L^2$ . As simulations tend to show that the radio emission is collimated, we also take into account a collimated emission scenario with an opening angle  $\theta = 1/\Gamma$  with  $\Gamma = 2$  and  $\Gamma = 10$ . In this case the radio beamed luminosity is  $L_{\text{beamed}} = L_{\text{radio}} \delta^n$  where  $\delta = \Gamma^{-1} (1 - \beta \cos \iota)^{-1}$ ,  $\beta = \sqrt{1 - \frac{1}{\Gamma^2}}$  with  $\iota$  as the inclination.

Similarly to the optical case, for the X-ray emission, we obtain the X-ray luminosity from the bolometric luminosity with the bolometric corrections provided in [5] and we claim the detection of the X-ray EM emission if  $F_X \geq 4 \times 10^{-17} \text{ erg s}^{-1} \text{ cm}^{-2}$ .

For the optical and X-ray emission, we also explore the role of obscuration. In both cases, the absorbed luminosity is the original luminosity in the corresponding band multiplied by a dumping factor. For example, in X-ray we define the absorbed luminosity as  $L_{X,\text{abs}} = L_X e^{-\tau_X}$  with  $\tau_X = \sigma_X N_H$  where  $\sigma_X$  is the X-ray cross section and  $N_H$  is the hydrogen column density. Similarly, in optical we can define  $\tau_{\text{opt}} = \sigma_{\text{opt}} N_{\text{dust}}$  where  $\sigma_{\text{opt}}$  is the optical cross section and  $N_{\text{dust}}$  is the dust column density (see [12] for more details).

### 3. Results

For the rest of the proceeding, we will refer to two models: *maximising* and *minimising*. In the former, AGN obscuration is negligible, the radio emission is isotropic and the binary emits in X-ray at Eddington. In the latter, the AGN is obscured, the radio emission has  $\Gamma = 2$  and the binary accretes in X-ray the reservoir gas.

In Fig. 1 we report the average number of mergers, MMcands and EMcps as function of redshift and chirp mass. Starting from the Q3d and Q3nd models, LISA can observe (i.e.  $\text{SNR} > 10$ ) the entire population, even if they are at very large redshift because the typical chirp mass is of the order of  $\mathcal{M} \simeq 10^{5-6} M_\odot$ . However, in the Pop3 scenario we lose 80% of sources, especially at high-redshift and  $\mathcal{M} < 10^3 M_\odot$  because LISA is not really sensitive in this portion of the parameter space.

All the systems with a detectable EM counterpart are located at  $z < 8$ , because the system must be close in order for the EM counterpart to be detected. Interestingly, the MMcands have large value of chirp mass, because binaries with large masses are expected to be surrounded by more gas and, as a consequence, the EM counterpart is brighter. We estimate 48.7 (24.4) [38] MMcands for Pop3 (Q3d) [Q3nd] in 4 years of LISA observation in the maximising scenario. However these numbers go down to 6.6 (3.6) [4.1] in the minimising one.

Including the final requirement on the sky localization, we can look at the number of EMcps. In particular, we predict 6.8 (14.9) [20.9] EMcps in 4 yr in the maximising model. AGN obscuration

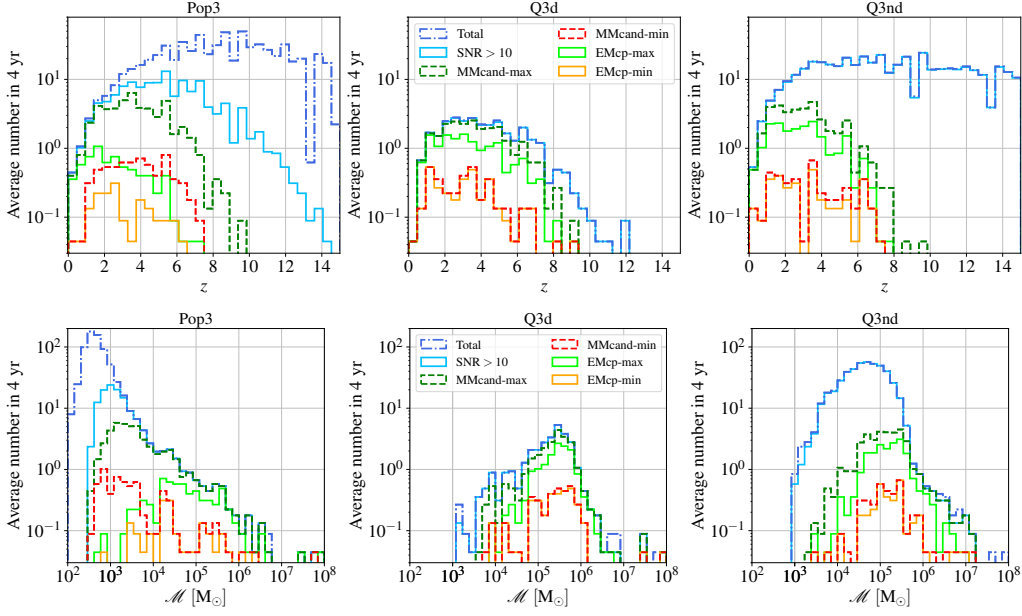


**Figure 1:** Redshift (upper panels) and chirp mass (lower panels) distributions for each astrophysical model. Dark blue dotted-dashed lines represent the astrophysical distributions; light blue solid lines represent the systems with SNR > 10. Light green and yellow solid lines correspond to the EMcps while the dark green and red dashed lines represent the MMcands.

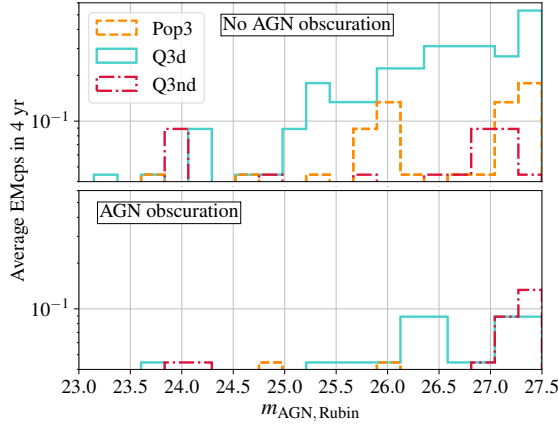


**Figure 2:** Magnitude distributions for the EMcps detected in optical with the Rubin Observatory, as specified by the legend.

and collimated radio emission play a significant role in reducing the number of EMcps and indeed we find 1.7 (3.4) [3.4] EMcps in the minimising model. For completeness, in Tab. 1 we report the total number of EMcps in all the scenarios considered.

In order to show the impact of AGN obscuration, in Fig. 2 we show the magnitude distributions for the EMcps detected in optical by the Rubin Observatory for the three astrophysical models. As expected the Q3d model provides the largest number of EMcps because these systems are the best localized by LISA and with the largest reservoir of gas to accrete. In the case without obscuration

(In 4 yr)	LSST, VRO	SKA+ELT			Athena+ELT		
		Isotropic	$\theta \sim 30^\circ$	$\theta \sim 6^\circ$	Catalog $F_{X, \text{lim}} = 4e-17$	Eddington $F_{X, \text{lim}} = 4e-17$	
	$\Delta\Omega = 10 \text{ deg}^2$			$\Delta\Omega = 0.4 \text{ deg}^2$	$\Delta\Omega = 0.4 \text{ deg}^2$		
No-obsc.	0.84	6.8	1.51	0.04	0.49	1.02	Pop3
	3.07	14.9	2.71	0.04	2.67	3.87	Q3d
	0.53	20.6	3.2	0.04	0.58	4.4	Q3nd
Obsc.	0.27	6.8	1.51	0.04	0.04	0.37	Pop3
	0.84	14.9	2.71	0.04	0.22	0.18	Q3d
	0.22	20.6	3.2	0.04	0.09	0.4	Q3nd

**Table 1:** Average number of EMcps for each observational configuration, assuming 4 yr of LISA mission.

**Table 2:** Number of *1mode*, *2modes* and *8modes* EMcps in 4 yrs of LISA observation, for the three astrophysical models and in the maximising case.

	<i>1mode</i>	<i>2modes</i>	<i>8modes</i>
Pop3	6.0	0.31	0.13
Q3d	10.7	3.9	0.18
Q3nd	16.8	3.5	0.4

(*maximising*), most of the EM counterparts are already faint and close to the lower limit for detection. If we take into account AGN obscuration, the number of EMcps decreases dramatically and only few events in the Q3d model survive.

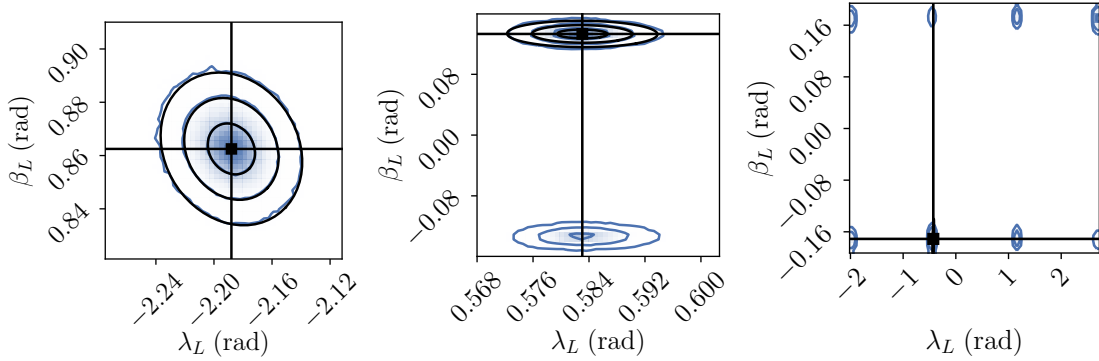


**Figure 3:** Example of sky localization distribution for *1mode* (left), *2modes* (middle) and *8modes* (right) binary systems. Blue contours represent the results of MCMC, black lines the fisher estimate and the black square the true binary position.

If we want to search for an EM counterpart, the sky localization is a crucial information that must be provided to telescopes. LISA ability to localize a system in the sky will depend on the intrinsic binary parameters (masses and redshift mostly) but also on the actual binary position in the sky. Depending on the combination of these values, the sky localization provided might vary

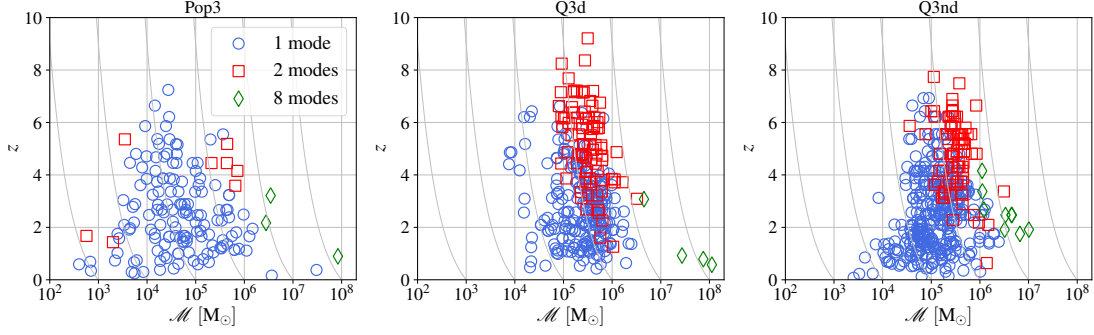


**Figure 4:** Scatter plot in the  $z - M$  plane for the *1mode* (blue circles), *2modes* (red squares) and *8modes* (green diamonds) EMcPs in the maximising case.

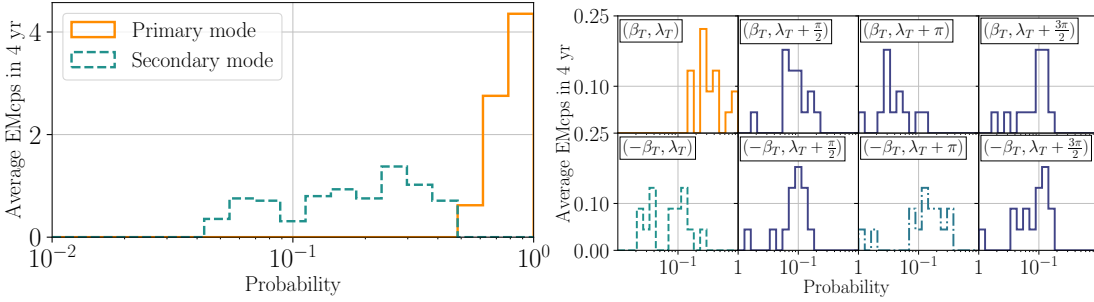


**Figure 5:** Left: Number of *2modes* EMcPs as function of the probability of the sky modes. Right: Number of *8modes* EMcPs as function of the probability of the eight sky position modes.

of several orders of magnitude [13]. Moreover, recent studies have highlighted the fact that the sky posterior distribution might appear multimodal in the sky due to degeneracies in the detector pattern function. These degeneracies can be broken by the orbital motion of the detector or by its high-frequency response. In Fig. 3 we report three examples: a *1mode* system with a single mode in the sky posterior distribution; a *2modes* system whose sky posterior distribution presents two mode symmetric respect to the plane of LISA and an *8modes* system with eight modes in the sky. In order to understand better where the degeneracies arise from, in Fig. 4 we report the distribution of *1mode*, *2modes* and *8modes* EMcPs in the  $z - M$  plane. It is clear that most events are unimodal, especially at low chirp mass and redshift where the combination of LISA motion and high-frequency response is sufficient to fully break the degeneracies. As we go to larger masses, we notice the appearance of the *2modes* systems because most of their signal is accumulated in the last days before merger and, in this case, LISA motion becomes irrelevant. Finally, the most massive systems are all *8modes* systems because, for these systems, even the high-frequency response does not contribute, coalescing at lower frequencies.

To quantify the role of multimodal events, in Tab. 2 we report the number of *1mode*, *2modes* and *8modes* EMcPs. While *8modes* do not contribute significantly to the rate of EMcPs, we find that *2modes* EMcPs represent the 5%, 26% and 17% of the total EMcPs for Pop3, Q3d and Q3nd.

However, another key information we have to take into account is the probability of these secondary modes. We evaluate the probability of secondary modes as the ratio between the number

of samples in a certain mode over the total number of samples. Interestingly, we find that for *2modes* systems the secondary mode contains always more probability than the secondary one, while for *8modes* systems, all the mode have similar probability. This result is reported in Fig. 5

#### 4. Conclusions

We have reported the latest predictions for the numbers of multimessenger events detectable by LISA and future EM facilities. We started from a population of MBHBs and computed the detectability of the EM emission at different wavelengths. We also performed the parameter estimation in order to get the information on the sky localization of the source.

Overall, we find that the EM counterpart to MBHB mergers can be observed up to  $z \sim 6 - 8$ . Without AGN obscuration and isotropic radio emission, we expect between 7 and 20 EMcps in 4 yr of LISA mission. However in the pessimistic case, these numbers go down to 2 – 3. We also find that the EM counterpart produced is faint, even for the future facilities, highlighting once again the need to accurately plan any follow-up strategy. Finally, systems whose sky posterior distribution is multimodal in the sky do not contribute significantly to the systems with a detectable EM counterpart.

#### References

- [1] P. Amaro-Seoane et al., arXiv:1702.00786 [astro-ph.IM]
- [2] M. Volonteri, *The Astronomy and Astrophysics Review* 18, 279 (2010), arXiv:1003.4404 [astro-ph.CO]
- [3] E. Barausse, *Monthly Notices of the Royal Astronomical Society* 423, 2533 (2012), arXiv:1201.5888 [astro-ph.CO]
- [4] S. Marsat et al., *Phys. Rev. D* 103, 083011 (2021), arXiv:2003.00357 [gr-qc].
- [5] X. Shen et al., *Monthly Notices of the Royal Astronomical Society* 495, 3252 (2020), arXiv:2001.02696 [astro-ph.GA].
- [6] A. Sesana et al., *Physical Review D* 83, 044036 (2011), arXiv:1011.5893 [astro-ph.CO]
- [7] P. Auclair et al., arXiv:2204.05434 [astro-ph.CO]
- [8] K. G. Arun et al., *Living Reviews in Relativity* 25, 4 (2022), arXiv:2205.01597 [gr-qc]
- [9] A. De Rosa et al., *New Astronomy Reviews* , 101525 (2020)
- [10] T. Dal Canton et al. , *Astrophysical Journal*, 886, 146 (2019), arXiv:1902.01538 [astro-ph.HE]
- [11] G. Lops et al., arXiv:2207.10683 [astro-ph.GA]
- [12] A. Mangiagli et al., arXiv:2207.10678 [astro-ph.HE].
- [13] A. Mangiagli et al., *Phys. Rev. D* 102, 084056 (2020), arXiv:2006.12513 [astro-ph.HE].